ISSN 1330–0008
CODEN FIZAE4

SYNCHROTRON X-RAY DIFFRACTION LINE PROFILE [1]

DAVOR BALZAR[a,c], PETER W. STEPHENS[b,d], and HASSEL LEDBETTER[a]

[a] *Materials Science and Engineering Laboratory, National Institute of Standards and Technology, 325 Broadway, Boulder, CO 80303, U. S. A.*
[b] *National Synchrotron Light Source, Brookhaven National Laboratory, Upton, NY 11973, U. S. A.*
[c] *On leave from X-ray Laboratory, Division of Materials Research and Electronics, Physics Department, Rudjer Bošković Institute, P.O. Box 1016, 10001 Zagreb, Croatia*
[d] *On leave from Physics Department, State University of New York, Stony Brook, NY 11794, U. S. A.*

Received 31 January 1997

UDC 538.95

PACS 61.10.-i

This paper is dedicated to Professor A. Bonefačić on the occasion of his 70th birthday

We analyse diffraction line profiles obtained at the X3B1 National Synchrotron Light Source powder-diffraction beamline. Calculated diffraction-line widths are compared to the measurements of a National Institute of Science and Technology Standard Reference Material, LaB_6. The discrepancy at high Bragg angles is probably caused by the inadequate Gaussian approximation for the Darwin width of monochromator Bragg reflection. The equatorial-slit width has a major influence not only on vertical (equatorial) divergence but also on the character of diffraction-line profiles at high angles. The least-squares fits of instrument-function deconvoluted tungsten-line profiles show that a Voigt function satisfactorily models physically broadened line profiles.

[1] Noncopyrightable U.S. government contribution.

1. Introduction

With the increasing use of synchrotron sources in condensed-matter physics and materials science, there is interest to better characterize some aspects of X-ray diffraction that are specific for the synchrotron radiation and focusing optics. In particular, precise knowledge of the angle-dispersive diffraction line-profile shape is of utmost importance in X-ray powder diffraction, especially in line-broadening analysis, Rietveld refinement [1], and other whole-powder-pattern fitting programs. In this regard, laboratory X-ray sources were investigated extensively, but synchrotron radiation remains inadequately characterized.

Material defects cause diffraction line broadening. Synchrotron radiation is inherently advantageous compared to laboratory sources for line-broadening studies for many reasons: naturally high beam collimation provides a superior resolution, the wavelength of the monochromatic beam can be easily tuned, and line shape is generally simpler and controlled to our preference. Most important, however, is the high resolution, that is, the narrow instrumental line profile implies a high sensitivity to small physical broadening.

The aim of this work is to analyse the basic aspects of X-ray diffraction line profiles obtained with synchrotron radiation. In particular, we focused on line shape caused by both instrumental factors and physical origins.

2. Experiment

Synchrotron-radiation measurements were performed on the X3B1 beamline at the National Synchrotron Light Source (NSLS), Brookhaven National Laboratory. The triple-axis parallel geometry is defined by a Si channel-111-cut monochromator, a flat specimen, and a Ge 111-cut analyzer crystal (see Fig. 1).

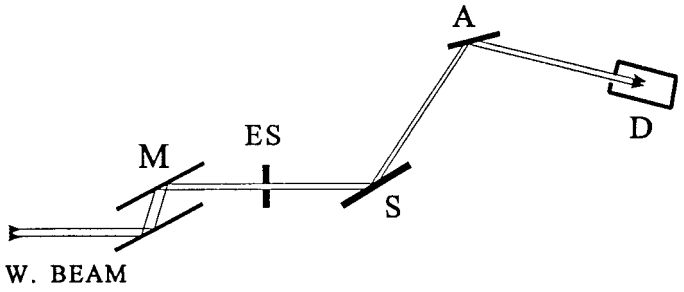

Fig. 1. Schematic view of X3B1 NSLS beamline in the equatorial plane: (M) channel-cut monochromator crystal; (ES) equatorial slit; (S) flat-plate specimen; (A) analyzer crystal; (D) proportional detector.

Diffraction lines are broadened for two reasons: Instrumental contribution g and physical (specimen) origins f (such as point, line, and extended lattice defects, small-angle and large-angle boundaries, etc.). The observed line profile is a convolution of these two

effects:

$$h(x) = g(x) \star f(x) + \text{background}. \tag{1}$$

Here, x represents the data-sampling variable (either Bragg angle θ or modulus of the scattering vector $q = 2(\sin\theta - \sin\theta_0)/\lambda$), where θ_0 corresponds to the diffraction-line centroid). Both wavelength distribution Ω and geometrical aberrations Υ contribute to the instrumental profile. They are treated as the characteristic of the particular instrument:

$$g(x) = \Omega(x) \star \Upsilon(x). \tag{2}$$

To obtain microstructural parameters of the specimen, the physically broadened profile f must be extracted from the observed profile h provided that the instrumental profile g is calculated or measured prior to the deconvolution. Measurements are performed on a suitable specimen that shows minimal physical (structural) broadening, such as NIST Standard Reference Material (SRM) LaB_6. Both laboratory and synchrotron diffraction line profiles are closely approximated with the Voigt function or its pseudo-Voigt and Pearson-VII approximations [2]. To compare measured and calculated instrumental profiles, we shall review the overall effects of geometrical aberrations on the synchrotron diffraction-line shape.

3. Synchrotron diffraction-line shape

Most of the diffraction line-profile models rely on a study of Caglioti, Paoletti, and Ricci [3] that was developed for neutron diffraction and later adapted to the synchrotron case [4]. Basic studies of synchrotron powder diffraction were undertaken by Cox et al. [5], who also gave a comprehensive review of the field [2].

The main equatorial instrumental factors affecting the diffraction-line profile can be summarized as follows:

(i) Source height (vertical angular distribution of the polychromatic beam) is approximated with the Gaussian function at the bending magnet. It depends on storage-ring electron (positron) relativistic factor γ, photon energy ε, and the critical photon energy ε_c (5.04 keV at NSLS):

$$g_S(z) = \exp\left(-\frac{4\ln 2 z^2}{\text{FWHM}_\phi^2}\right), \tag{3}$$

where the vertical (equatorial, for it is in the scattering plane) divergence is

$$\text{FWHM}_\phi = \frac{1.331}{\gamma(\varepsilon_c/\varepsilon)^{0.425}}; \quad \gamma = [1-(v/c)^2]^{-1/2} = E/(m_0c^2). \tag{4}$$

Here, v, E and m_0 are the electron (positron) speed, energy, and rest mass, respectively, and c is the speed of light.

(ii) Slit width a:

$$g_{\mathrm{ES}}(z) = \begin{cases} 1 & |z| \le a/2 \\ 0 & |z| > a/2 \end{cases} \tag{5}$$

(iii) Monochromator and analyzer (perfect) crystal normalized Darwin Bragg-reflection shape [6] (rocking curve):

$$g_{\mathrm{M,A}}(z) = \frac{s^2}{[z \pm (z^2 - s^2)^{1/2}]^2}. \tag{6}$$

Here, s defines the region for a perfect reflection (without absorption) from a crystal.

The most important axial aberration is a divergence, which causes asymmetry at low angles. This effect must be modeled separately and will not be treated here. For a mathematical model to correct the line profiles for axial divergence see the recent paper by Finger, Cox and Jephcoat [7].

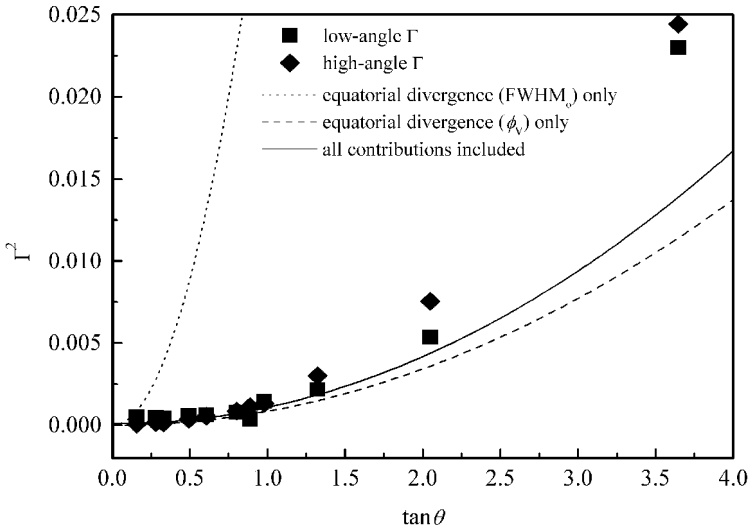

Fig. 2. Full width at half maximum (FWHM) Γ *of split-Pearson-VII funtions fit to the line profiles of* LaB_6 *(full squares and diamonds). Different broadening contributions to (10) are presented with lines.*

The total diffraction-line profile results from a convolution of all the contributions, which has to be calculated numerically. However, for most purposes, a simple estimation of line widths as a function of diffraction angle may suffice. Wavelength dispersion follows from the Bragg law:

$$\Delta\lambda/\lambda = (\omega_{\mathrm{M}}^2 + \omega_{\mathrm{A}}^2 + \mathrm{FWHM}_{\phi}^2)^{1/2} \cot\theta. \tag{7}$$

Here, the shape of Darwin–Bragg reflection is approximated with the Gaussian function. ω_{M} and ω_{A} designate monochromator and analyzer-crystal Darwin widths. They depend

on the structure factor, polarization, absorption, and temperature (see for instance Warren [6]).

To recognize the relative importance of various contributions, we estimate the angular resolution at the X3B1 NSLS beamline with 8 keV photon energy, that is, approximately at the Cu Kα wavelength:

$$\mathrm{FWHM}_\phi(2.5\ \mathrm{GeV}, 8\ \mathrm{keV}) = 0.0190^\circ; \tag{8}$$

$$\omega_\mathrm{M}(111\ \mathrm{Si}, 8\ \mathrm{keV}) = 0.0021^\circ; \qquad \omega_\mathrm{A}(111\ \mathrm{Ge}, 8\ \mathrm{keV}) = 0.0045^\circ.$$

It seems that Darwin widths of both analyzer and monochromator crystals make a minor contribution and can be neglected in the first approximation. However, this large a divergence would yield very poor resolution (see Fig. 2) and it must be controlled by the narrow equatorial slit in front of the specimen. The FWHM_ϕ yields the height of the beam at the slit position of about 4.5 mm for the X3B1 beamline (ring–slit distance is 13.7 m). Usually, at least three times narrower slit has to be used to improve the resolution. For instance, we collected the LaB_6 data at 0.130049(3) nm with 0.75 mm equatorial-slit width (Fig. 2). Line profiles were fitted with a split–Pearson VII function to model the peak-asymmetry effects. The main peak-width contributions are then

$$\phi_\mathrm{V} = 0.0031^\circ; \tag{9}$$

$$\omega_\mathrm{M}(111\ \mathrm{Si}, 9.54\ \mathrm{keV}) = 0.0015^\circ; \quad \omega_\mathrm{A}(111\ \mathrm{Ge}, 9.54\ \mathrm{keV}) = 0.0032^\circ.$$

Here, the vertical divergence ϕ_V is defined by the equatorial slit. Certainly, the monochromator and analyzer Darwin widths become significant factors. To calculate the FWHM, we use the expression of Sabine [4]:

$$\begin{aligned}\Gamma^2 = {} & \phi_\mathrm{V}^2 \left(\frac{2\tan\theta}{\tan\theta_\mathrm{M}} - \frac{\tan\theta_\mathrm{A}}{\tan\theta_\mathrm{M}} + 1 \right)^2 \\ & + \omega_\mathrm{M}^2 \left(\frac{2\tan\theta}{\tan\theta_\mathrm{M}} - \frac{\tan\theta_\mathrm{A}}{\tan\theta_\mathrm{M}} - 1 \right)^2 + \omega_\mathrm{A}^2 \\ & + (w_\mathrm{ES}^2 + w_\mathrm{RS}^2/D_\mathrm{SR}^2)/12.\end{aligned} \tag{10}$$

Here, we add the influence of specimen size (which approximately equals the equatorial-slit width w_ES) and receiving-slit width w_RS (it can be neglected when the analyzer crystal is used), where D_SR is the specimen to receiving-slit distance.

In Fig. 2 we plot three curves: the equatorial divergence term given by FWHM_ϕ, the first term of (10), and all terms of (10). The monochromator-related wavelength (energy) dispersion has a major influence at high diffraction angles, but the analyzer as well as slit contributions are quite small, except at low angles. The fit is satisfactory up to about

$2\theta = 110°$. At high angles, (10) may be inadequate because it assumes that the transmission functions of all optical elements that contribute to broadening follow a Gaussian distribution. That may be a fair approximation in neutron-diffraction case, but certainly not for synchrotron-radiation diffraction, where profiles have a significant Lorentzian contribution. To further examine this matter, in Fig. 3 we show the Voigt-function fits to the LaB_6 line profiles so that Lorentzian and Gaussian parts are separated. From Fig. 2 is evident that the major influence on peak width comes from the equatorial divergence of the beam and

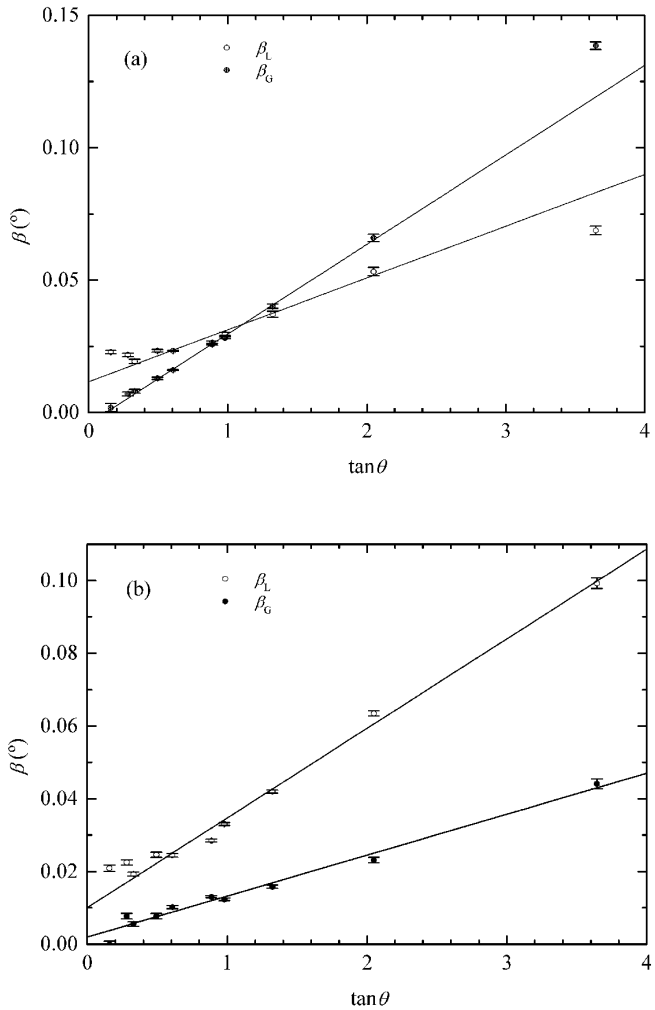

Fig. 3. Lorentz- (β_L) and Gauss- (β_G) integral breadths of the Voigt-function fits to the LaB_6 *line profiles. The data were collected at 0.130049(3)* nm*: (a) 0.75* mm *equatorial slit; (b) 0.25* mm *equatorial slit.*

wavelength dispersion at the monochromator. Although the equatorial-beam distribution (3) may have a substantial Lorentzian contribution, which would cause discrepancy at large angles, the latter effect is dominant at larger angles for this monochromator (channel-cut) configuration. It is likely that long tails of the shape of monochromator Bragg reflection (see (6)) contribute substantially to the peak width and are visible as a Lorentzian part of fitting Voigt or a similar function. This is confirmed by the measurements with narrower equatorial slit (0.25 mm), presented in Fig. 3b. The obvious difference from measurements with the 0.75 mm slit (Fig. 3a) is a dominant Lorentzian character of the profiles at large angles. Therefore, a wider equatorial slit has an effect of cutting off the long tails characteristic of the reflection from the monochromator. This effect may be more significant in constant-wavelength neutron diffraction, where wider slits must be used because of generally poor beam intensities, resulting in predominantly Gaussian peaks.

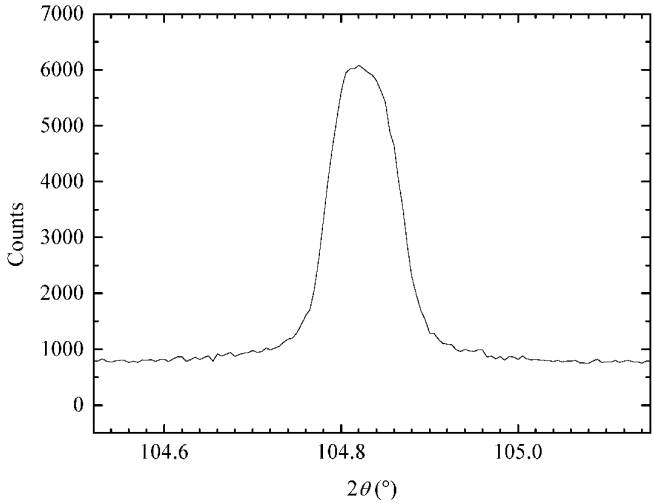

Fig. 4. The LaB_6 *line profile (Bragg reflections from the* (843), (922), (850) *and* (762) *planes coincide at this diffraction angle) recorded at 0.069839(2)* nm *with the 1.5* mm *equatorial slit.*

How slits can affect the line profiles is illustrated in Fig. 4. The measurement of the LaB_6 reflection was made with 1.5 mm wide equatorial slit. The peak has the appearance of a "super-Gaussian". It is clear that the source height (3) is modulated by the slit function (5). The resulting profile is a convolution:

$$g_S \star g_{ES} = \int_{-a/2}^{a/2} \exp[-b^2(x-z)^2]\mathrm{d}z = \frac{\sqrt{\pi}}{2b}[\mathrm{erf}(b\frac{a}{2} - bx) + \mathrm{erf}(b\frac{a}{2} + bx)], \qquad (11)$$

where

$$b^2 = \frac{4\ln 2}{\mathrm{FWHM}_\phi^2}. \qquad (12)$$

If the slit width a is smaller than the FWHM_ϕ, the profile stays approximately Gaussian, but there is a loss of integrated intensity. If the slit width is increased substantially over the FWHM_ϕ, (11) approaches the constant value of $\sqrt{\pi}/b$, thus making a rectangular-like profile shape. However, there is an advantage in a substantial increase of integrated intensity that may outweigh the drawbacks. Moreover, if the specimen shows even a small amount of physical line broadening, the "super-Gaussian" line shape will not be obvious because the physically broadened line profile will smear it out.

4. Physically broadened line profiles

From (1), it follows that deconvolution can be performed in terms of complex Fourier transforms of respective functions:

$$F(n) = \frac{H(n)}{G(n)}. \tag{13}$$

The inverse Fourier transform gives a physically broadened line profile by a summation over all the harmonic numbers n:

$$f(x) = \sum_n \frac{H(n)}{G(n)} \exp\left(-\frac{2\pi \mathrm{i} x n}{x_m}\right). \tag{14}$$

Hence, the physically broadened profile f is retrieved from the observed profile h without any assumption (bias) on the peak-profile shape. However, (13) may not give a solution if the Fourier coefficients of the f profile do not vanish before those of the g profile. Furthermore, if physical broadening is small compared with instrumental broadening, deconvolution becomes too unstable and inaccurate. Alternatively, it is advantageous to approximate the physically broadened line profile with an analytical function, and perform the convolution process with a predetermined instrumental profile according to (1), which is always a mathematically stable procedure. Moreover, a subsequent line-broadening analysis of physically broadened line profile is much simpler if an analytical approximation is adopted. However, it is necessary to validate whether the physically broadened line profile can be approximated successfully with any common analytical function. For this purpose we prepared a "standard" tungsten specimen that shows a particular amount of physical broadening. The specifics about specimen preparation and data collection and analysis were published elsewhere [8].

Deconvolution was performed following (13) with $\mathrm{LaB_6}$ profiles defining the instrumental function G. Because of noise in the raw data, Fourier coefficients become unreliable after some harmonic number, and cause large oscillations in the synthesized profiles. As an illustration, a typical plot of a synthesized physically broadened line profile, obtained from the laboratory X-ray data, is shown in Fig. 5a (110 tungsten Bragg reflection). Conversely, the same physically broadened line profile obtained from the synchrotron data, with approximately identical counting statistics, does not show peak-tail ripples. It indicates that the generally superior synchrotron resolution and a simpler (singlet) wavelength distribution allows for more precise line-broadening studies. The fact that the synchrotron 110 tungsten deconvoluted profile (Fig. 5b) is perfectly symmetrical while its laboratory

counterpart (Fig. 5a) is not, although the peak asymmetry is much more pronounced for the synchrotron source at smaller angles because of large axial-divergence effect, shows that the Cu Kα doublet seriously affects deconvolution and, consequently, all the derived parameters.

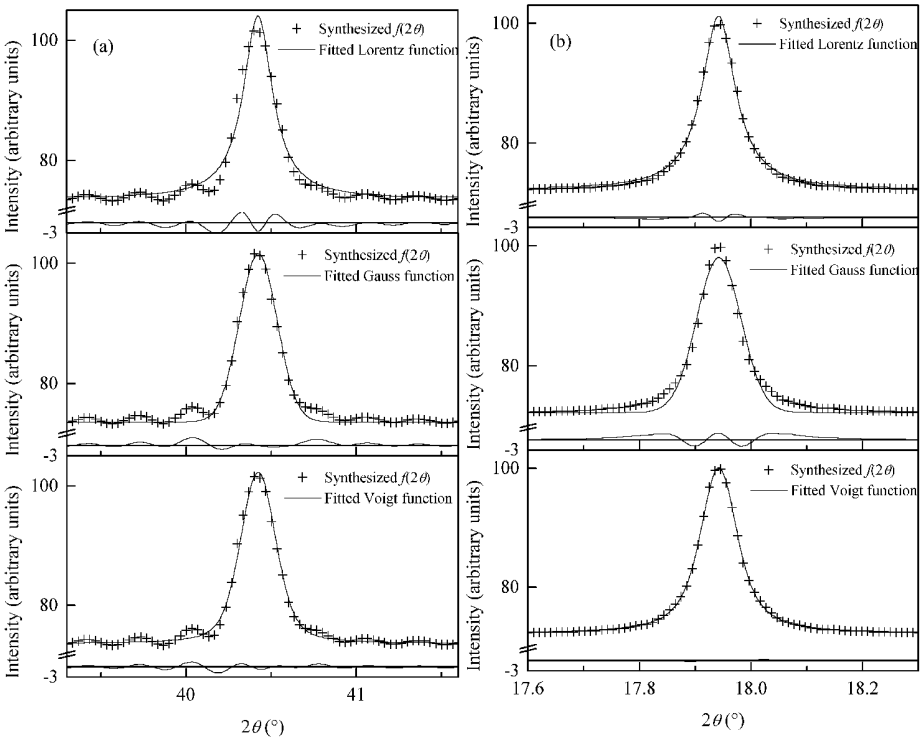

Fig. 5. Lorentz-, Gauss-, and Voigt-function fits to the instrument-function deconvoluted physically broadened 110 tungsten diffraction-line profile. Difference patterns plotted around zero intensity on the smaller scale: (a) laboratory data; (b) synchrotron data.

To test whether simple analytical functions can successfully approximate a physically broadened profile, least-squares fits of Lorentz-, Gauss-, and Voigt-functions to the tungsten profiles were performed (see, for example, Fig. 5b). It is obvious that the Voigt function shows a superior and overall satisfactory fit. Even more important is how different functions fit profiles. Although the Lorentz-function approximates tails quite well, it fails to fit profile shape close to its maximum. On the contrary, the Gaussian function fits fairly well around the peak maximum, whereas tails fall off too rapidly. This is known to be also true for the observed diffraction profiles. Despite substantial profile-tail ripples, the fits of physically broadened profiles obtained from the laboratory data (Fig. 5a) show the same behavior.

These measurements show that the physically broadened line profile can be satisfactorily approximated with a Voigt function. Then, the subsequent line-broadening analysis can be performed in a simpler manner [9].

5. Conclusions

Synchrotron radiation is certainly superior to laboratory X-ray sources for diffraction purposes. Generally, a larger number of optical elements along the beamline gives the user more flexibility but also poses more challenge.

For usual operating conditions, the contribution of monochromator Darwin width should not be neglected, especially at large angles.

The summary instrumental function (assumed to be represented closely with the measured LaB_6 line profiles) contains a significant Lorentzian contribution, which is incompatible with the presumption that all transmission functions are approximated with Gaussian functions. The most likely reason why (10) fails to model diffraction-line width at large angles is because the monochromator perfect-Bragg reflection cannot be approximated with a Gaussian function.

Physically broadened line profiles of a suitably prepared tungsten powder are approximated satisfactorily with a Voigt function.

References

1) H. M. Rietveld, Acta Cryst. **22** (1967) 151;

2) D. E. Cox, in *Handbook on Synchrotron Radiation, V.* **3**, Edited by G. S. Brown and D. E. Moncton, North-Holland, New York, 1991, p. 155;

3) G. Caglioti, A. Paoletti, and F. P. Ricci, Nucl. Instrum. Methods **3** (1958) 223;

4) T. M. Sabine, J. Appl. Crystallogr. **20** (1987) 173;

5) D. E. Cox, J. B. Hastings, W. Thomlinson and C. T. Prewitt, Nucl. Instrum. Methods **208** (1983) 573;

6) B. E. Warren, *X-ray Diffraction*, Dover Publications, New York, 1990, p. 324;

7) L. W. Finger, D. E. Cox and A. P. Jephcoat, J. Appl. Crystallogr. **27** (1994) 892;

8) D. Balzar, in *Microstructure Analysis from Diffraction,* edited by R. L. Snyder, H. J. Bunge and J. Fiala, International Union of Crystallography (1997) in press;

9) D. Balzar and Hassel Ledbetter, J. Appl. Crystallogr. **26** (1993) 97.

PROFIL SINHRONTRONSKE RENGENSKE DIFRAKCIJSKE LINIJE

Analizirali smo difrakcijske profile linija dobivenih na snopu X3B1 Nacionalnog sinhrotronskog izvora svjetlosti u Brookhavenu. Načinili smo usporedbe za razne uvjete i s vi vse prilagodbenih funkcija. Prilagodbe primjenom najmanjih kvadrata za profile volframovih linija, koje su bile dekonvoluirane instrumentalnom funkcijom, pokazuju da Voigtova funkcija dobro opisuje fizičko proširenje profila linija.